High-performance X-ray Imaging Enabled by *In-situ* Recrystallized Antimony(III)-based Halide Glass-ceramics

Haixia Cui,[a] Guanyu Yan,[a] Wanjiao Li,[a] Xueqin Du,[a] Jinshuo Liu,[a] Shujuan Liu,[*a] and Qiang Zhao[*a,b]

[a] State Key Laboratory of Flexible Electronics (LoFE) & Institute of Advanced Materials (IAM), Nanjing University of Posts & Telecommunications, 9 Wenyuan Road, Nanjing 210023, Jiangsu, China.

[b] School of Physics and Optoelectronic Engineering & School of Chemistry and Materials Science, Nanjing University of Information Science and Technology, Nanjing 210044 Jiangsu, China.

*Correspondence: iamsjliu@ njupt.edu.cn; iamqzhao@njupt.edu.cn

Materials: 1,3-dicyclohexyl imidazolium (DCI) chloride and antimony trichloride ($SbCl_3$, 99.9%) were obtained from Aladdin. Acetonitrile (ACN) and ether were purchased from Sinopharm Chemical Reagent Co., Ltd. (China).

Synthesis of crystal: First, 1,3-dicyclohexyl imidazolium chloride (0.1 mmol) and $SbCl_3$ (0.1 mmol) were dissolved in ACN (2 mL). Subsequently, the ether used as counter-solvent slowly volatilized into the above-mentioned solution to obtain the block and transparent crystals.

Fabrication of glass: The glass was fabricated using a melt-quenching method. First, crystals were thoroughly ground into a fine powder and placed onto a quartz substrate. The substrate was then transferred to a heating stage and heated at 500 K until the powder was fully molten, forming a uniform melt. Finally, it was rapidly removed from the heating stage and allowed to cool naturally to room temperature, yielding a transparent glass.

Fabrication of glass-ceramic: The glass-ceramic was prepared via *in-situ* recrystallization by subjecting the glass to annealing on a heating stage at 350 K. This temperature lies below the peak crystallization temperature, ensuring sufficient crystallization while preventing excessive grain growth. The sample was then naturally cooled to room temperature, yielding a transparent glass-ceramic.

Computational Details: The melt-quenching process and in-situ recrystallization were simulated using ab initio molecular dynamics (AIMD) with the Vienna Ab initio Simulation Package (VASP). The computational model consisted of a 1 × 1 × 1 supercell containing 248 atoms (excluding CH_3CN molecules), with cell parameters of a = 16.9893 Å, b = 16.9893 Å, c = 33.1773 Å, α = 90°, β = 90°, and γ = 120°. All simulations were performed under the canonical ensemble (NVT), ensuring constant particle number, volume, and temperature. Simulations were conducted at 300, 600, 900, and 1200 K for a total of 20 ps, with the last 10 ps of each trajectory used to analyze the equilibration process. The glass was obtained by quenching the molten $(DCI)_3SbCl_6$ system from 900 K to 300 K over 9 ps; the glass-ceramic state was subsequently achieved through the formation of a heterojunction-like structure to optimize its properties. Radial distribution functions (RDFs) for Sb-Cl and Sb-N bonds were

computed during the melting phase. From the width of the first RDF peak, the generalized Lindemann ratio was subsequently determined following established methodologies.

Calculation of radiative/nonradiative transition rates

The radiative transition rates (k_r) and nonradiative transition rates (k_{nr}) were calculated with the following equations:

$$k_r = \frac{PLQY}{\tau} \#(1)$$

$$k_{nr} = \frac{1}{\tau} - k_r \#(2)$$

where PLQY is the photoluminescence quantum yield and τ is the decay time.

Calculation of Huang-Rhys factor

S (Huang-Rhys factor) represents the hardness or softness of the crystal lattice. A large S represents a soft crystal lattice and means a strong lattice vibration, which can be evaluated from the follow equation:

$$FWHM = 2.36\sqrt{S}\hbar\omega_{phonon}\sqrt{\coth\frac{\hbar\omega_{phonon}}{2k_BT}} \#(3)$$

where $\hbar\omega_{phonon}$ represents phonon frequency, k_B is the Boltzmann constant, and T is the temperature.

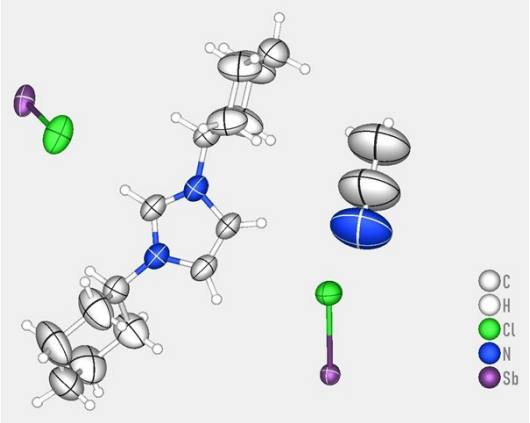

Fig. S1 Oak ridge thermal ellipsoid plot drawing of the crystal structure.

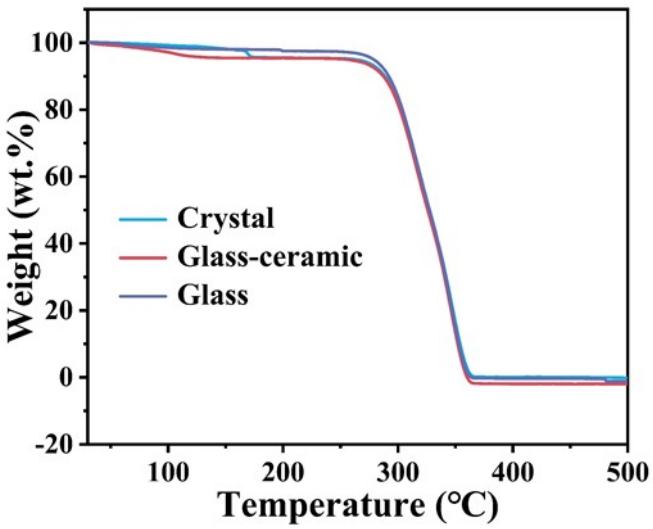

Fig. S2 TGA of crystals, glass-ceramic and glass, respectively.

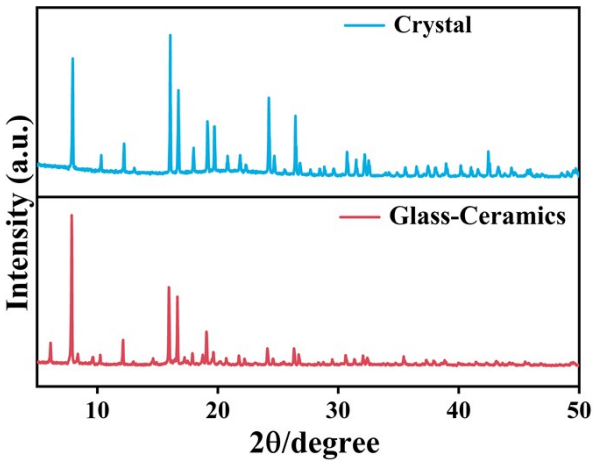

Fig. S3 PXRD of crystals and glass-ceramics.

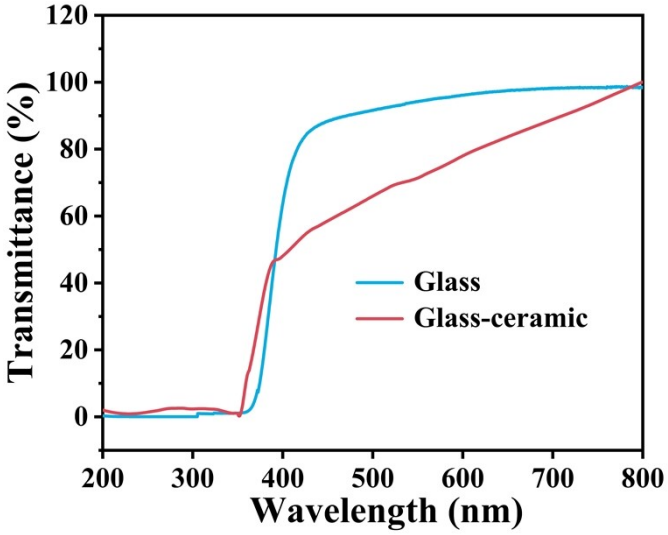

Fig. S4 The ultraviolet transmittance spectra of glass and glass-ceramics, respectively.

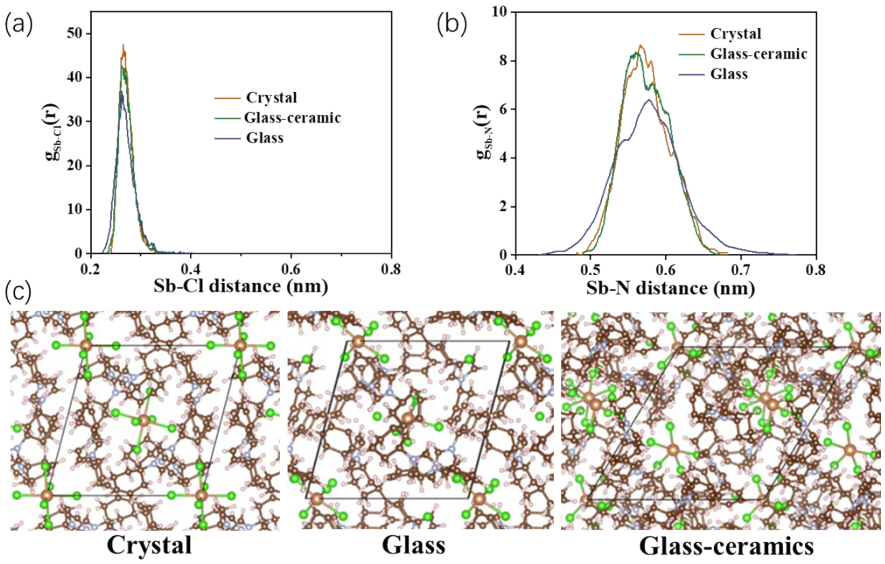

Fig. S5 (a) Partial RDFs gij(r) for (a) Sb-Cl distance and (b) Sb-N distance at different states (crystal, glass and glass-ceramics); (c) Structure at different states (crystal, glass and glass-ceramics).

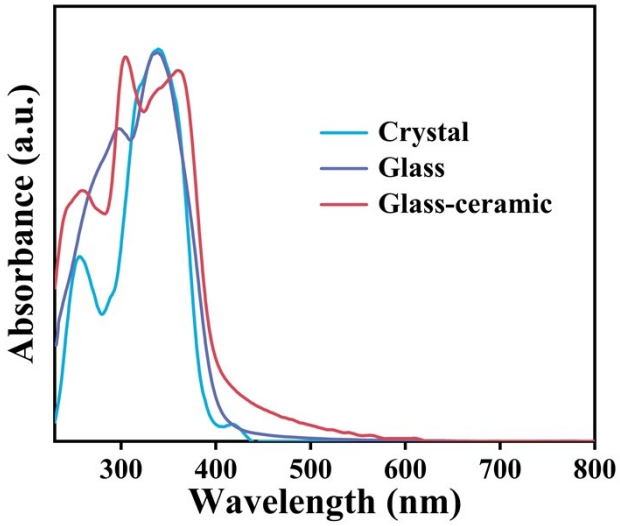

Fig. S6 The UV-Vis absorption spectra of glass and glass-ceramics, respectively.

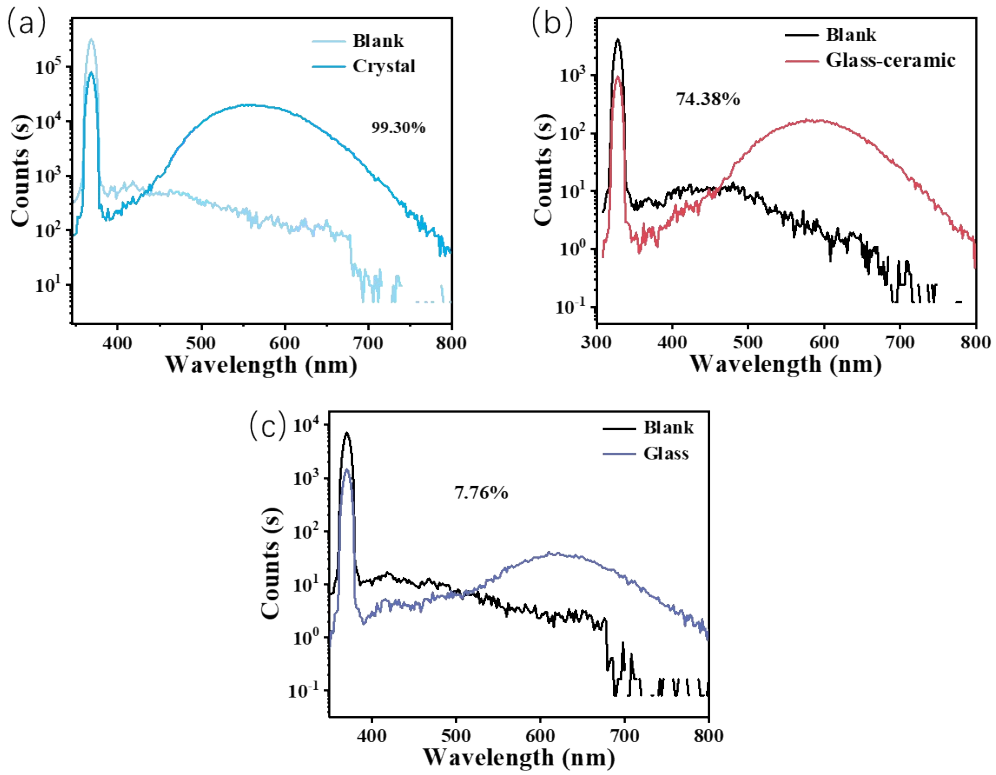

Fig. S7 The PLQYs of (a) crystal; (b) glass-ceramic; (c) glass.

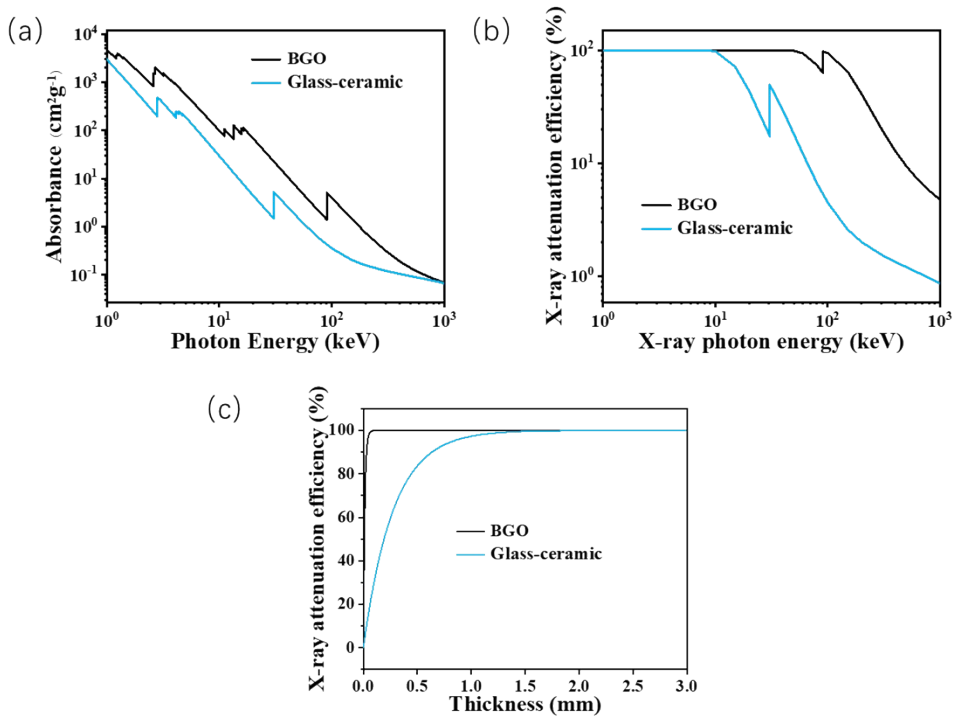

Fig. S8 (a) The absorption coefficients versus X-ray photon energy; (b) The curves of the attenuation efficiency versus thickness; (c) The curves of the attenuation efficiency versus X-ray photon energy for BGO and glass-ceramics.

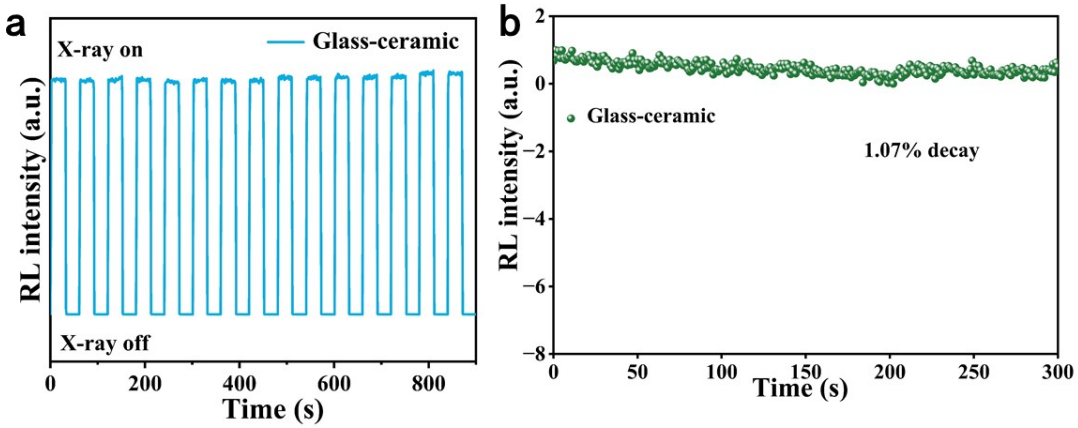

Fig. S9 Irradiation stability of the glass-ceramic scintillation screen under (a) discontinuous and (b) continuous X-ray exposure.

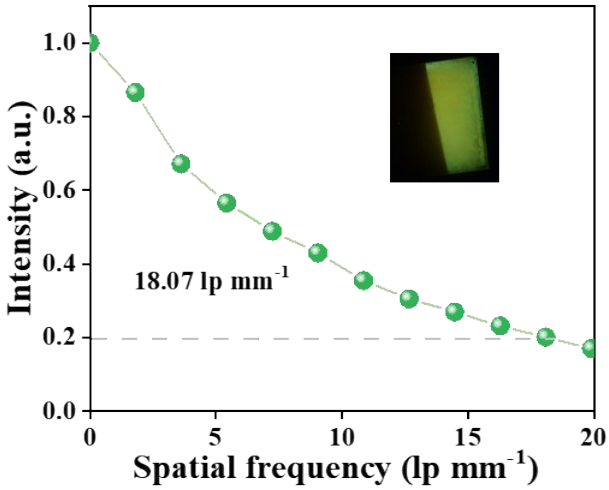

Fig. S10 MTF curve of the glass-ceramic scintillator screen.

Table S1. Detailed single crystal X-ray data of $(DCI)_3SbCl_6 \bullet CH_3CN$.

Identification code	$(DCI)_3SbCl_6$
Chemical Formula	$C_{47}H_{78}Cl_6N_7Sb$
Formula Weight	1075.61
Crystal System	trigonal
Space Group	R-3
a (Å)	16.9893
b (Å)	16.9893
c (Å)	33.1773
α (°)	90
β (°)	90
γ (°)	120
V (Å^3)	8293.2(7)
Z value	6
D(calcd) (g cm^{-3})	1.292
Temperature (*K*)	273.15
F(000)	3372.0
μ (mm^{-1})	0.826
R_1/wR_2, [I>2σ(I)]	R_1 = 0.0434, wR_2 = 0.1290
R_1/wR_2, [all data]	R_1 = 0.0548, wR_2 = 0.1345
GOF	1.103

Table S2. Selected bond lengths of $(DCI)_3SbCl_6 \bullet CH_3CN$.

Bond	Length/Å
Sb1-Cl1[1]	2.668
Sb1-Cl1	2.668
Sb1-Cl1[2]	2.668
Sb1-Cl1[3]	2.668
Sb1-Cl1[4]	2.668
Sb1-Cl1[5]	2.668

Table S3. Selected bond angles of $(DCI)_3SbCl_6 \bullet CH_3CN$.

Bond	Angle/°
$Cl1^1$ Sb1 $Cl1^2$	93.37(3)
$Cl1^3$ Sb1 $Cl1^4$	93.36(3)
$Cl1^3$ Sb1 $Cl1^5$	93.36(3)
Cl1 Sb1 $Cl1^4$	86.64(3)
$Cl1^2$ Sb1 $Cl1^5$	86.64(3)
$Cl1^1$ Sb1 Cl1	93.36(3)
$Cl1^2$ Sb1 $Cl1^3$	86.63(3)
$Cl1^1$ Sb1 $Cl1^5$	86.64(3)
Cl1 Sb1 $Cl1^3$	86.64(3)
$Cl1^2$ Sb1 Cl1	93.36(3)
$Cl1^1$ Sb1 $Cl1^4$	86.63(3)
$Cl1^4$ Sb1 $Cl1^4$	86.63(3)

Table S4. Summary of the photophysical parameters.

	Crystal	Glass-Ceramics	Glass
Lifetime (μs)	1.64	1.27	1.12
PLQY (%)	99.30	74.38	7.76
k_r	0.6055	0.5857	0.0693
k_{nr}	0.0043	0.2017	0.8236

Table S5. Summary of the spatial resolution for the state-of-the-art scintillator screen.

Compound	Resolution (lp mm^{-1})	Ref.
TEBA-2	10.4	J. Mater. Chem. C, 2024, 12, 12325
$(PPN)_2SbCl_5$	-	ACS Materials Lett., 2020, 2, 633
$[Bmmim]_2SbCl_5$	12.5	ACS Materials Lett., 2023, 5, 2481
$[FPPP]_2SbCl_7$	13.01	Inorg. Chem. Front., 2024, 11, 5034
$(NYP)_2SbCl_5$	7.77	Inorg. Chem. Front., 2024, 11, 522
(MTP_2SbCl_5)	10.2	Laser Photonics Rev., 2025, 19, 2401703
$C_{38}H_{36}P_2Sb_2Cl_8$	8.15	Adv. Funct. Mater., 2025, 35, 2412597
$C_{50}H_{44}P_2SbCl_5$	8.2	Laser Photonics Rev., 2023, 17, 2201007
$(BPP)_2SbCl_5$ 0.5 H_2O	13-14	Light Sci. Appl., 2026, 15, 88
$Cs_3Cu_2I_5$-AAO	10.4	Adv. Optical Mater., 2021, 9, 2101194
$[BzTPP]_2Cu_2I_4$	7	Laser Photonics Rev. 2023, 17, 2300427
$[AEPipz]CuBr_3 \cdot Br \cdot H_2O$	17.4	ACS Appl. Mater. Interfaces, 2024, 16, 41165
β-$Cs_3Cu_2Cl_5$	9.6	Nanoscale, 2021, 13, 19894
R/S-$[(L)_2MnBr]Br$	11.9	Adv. Optical Mater., 2024, 12, 2302185
$(DCI)_3SbCl_6 \cdot CH_3CN$	18.07	This work